Functional Materials Letters
Vol. 1, No. 1 (2008) 1–4

ENERGETIC AND THERMAL PROPERTIES OF TILT GRAIN BOUNDARIES IN GRAPHENE/HEXAGONAL BORON NITRIDE HETEROSTRUCTURES

MINGCHAO WANG[†], GUANGPING ZHANG[‡], HUISHENG PENG[§] and CHENG YAN[†,*]

[†]*School of Chemistry, Physics and Mechanical Engineering, Science and Engineering Faculty, Queensland University of Technology, Brisbane, QLD 4001, Australia*

[‡]*Shenyang National Laboratory for Materials Science, Institute of Metal Research, Chinese Academy of Sciences, 72 Wenhua Road, Shenyang 110016, China*

[§]*State Key Laboratory of Molecular Engineering of Polymers, Department of Macromolecular Science, and Laboratory of Advanced Materials, Fudan University*

[*]*c2.yan@qut.edu.au*

Received Day Month Year; Revised Day Month Year

Graphene/hexagonal boron nitride (G/h-BN) heterostructure has attracted tremendous research efforts owing to its great potential for applications in nano-scale electronic devices. In such hybrid materials, tilt grain boundaries (GBs) between graphene and h-BN grains may have unique physical properties, which have not been well understood. Here we have conducted non-equilibrium molecular dynamics simulations to study the energetic and thermal properties of tilt GBs in G/h-BN heterostructures. The effect of misorientation angles of tilt GBs on both GB energy and interfacial thermal conductance are investigated.

Keywords: Graphene; hexagonal boron nitride; heterostructure; tilt grain boundary; interfacial thermal conductance.

Graphene and hexagonal boron nitride (h-BN) have similar honeycomb-lattice structures, with only 2% lattice constant difference. Despite the structural similarity, they have totally different electronic properties. For instance, graphene possesses anomalous quantum Hall effect and high carrier mobility at room temperature[1-3] that offer novel applications in nano-devices. While a single-layer h-BN is an insulator with a wide bandgap energy of ~5.9 eV,[4-6] which is very promising for applications in optoelectronic devices[4] and field-effect transistors.[7, 8] Recently, research efforts have been devoted to explore the possibility of creating Graphene/h-BN (G/h-BN) heterostructures for broader applications such as atomically thin integrated circuitry. In fact, experimental studies have developed some synthesis methods, such as 'patterned regrowth', which can produce in-plane G/h-BN heterostructures with precisely controlled domain sizes.[9-11]

In these heterostructures, grain boundaries between graphene and h-BN grains are of particular interest, since they can remarkably influence the overall electronic properties. For instance, first principle calculations have predicted that in-plane G/h-BN interfaces (grain boundaries) may have variable bandgap,[12, 13] half-metallic behavior[12] and different electronic structures.[14] However, to date, there is almost no research on the energetic and thermal properties of tilt grain boundaries (GBs) in G/h-BN heterostructures. In this work, we investigated on both GB energy and thermal transport across tilt GBs in G/h-BN heterostructures using molecular dynamics simulations. To model the thermal transport, heat flux J_Q is introduced through the tilt GBs, causing a discontinuous temperature drop ΔT between the graphene and h-BN monolayers. The associated thermal boundary resistance R_κ (also called the Kapitza[15]), or equivalently the interfacial thermal conductance, $G_\kappa=1/R_\kappa$, can be evaluated via

$$J_Q = -G_\kappa \Delta T \tag{1}$$

As for the thermal conductivities κ of graphene and h-BN grains, they can be calculated on the basis of Fourier's law,

$$J_Q = -\kappa\left(\Delta T/\Delta z\right) \tag{2}$$

where $\Delta T/\Delta z$ is the temperature gradient.

In this work, we compute the thermal conductivity and interfacial thermal conductance using the reverse non-

equilibrium molecular dynamics (RNEMD) simulations.[16-18] According to the Müller-Plathe algorithm,[19] heat source and heat sink are placed at the center and at each end of G/h-BN heterostructures (Fig. 1), respectively, to generate a constant heat flux.

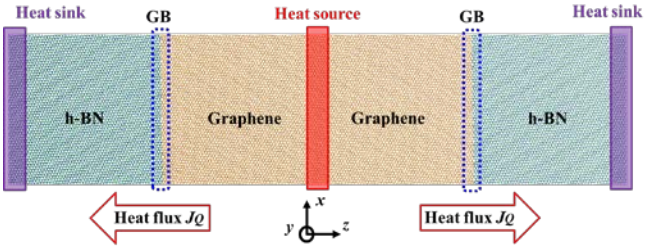

Fig. 1. The model of G/h-BN heterostructure for RNEMD simulations.

Tilt GBs in G/h-BN heterostructures comprise arrays of pentagon-heptagon (5-7) rings with different ring orientation angles and densities depending on the misorientation angles. Fig. 2 displays two regular types of GBs. Fig. 2(a1)-(g1) show the structures of zigzag-oriented GBs with initial misorientation angles, θ_{zigzag}, ranging from 0° to 21.8°. Fig. 2(a2)-(g2) show the structures of armchair-oriented GBs with initial misorientation angles, $\theta_{armchair}$, ranging from 0° to 27.8°. Generally, there is a relation between zigzag and armchair misorientation angles

$$\theta_{armchair} = 60^{\circ} - \theta_{zigzag} \tag{3}$$

Accordingly, for G/h-BN armchair-oriented GBs, a higher value of θ_{zigzag} implies a lower value of $\theta_{armchair}$ and a lower density of 5-7 rings. Here we only consider the thermal properties of G/h-BN heterostructures with respect to zigzag misorientation angles θ_{zigzag}. For structural dimensions, only graphene and h-BN grain sizes of 25 nm with widths of 12 nm along the GB direction are taken into account. Periodic boundary conditions are applied in both *x* and *z* directions. Two modified versions of Tersoff potentials are adopted to simulate the C-C interaction,[20] and C-B-N interaction.[21, 22] These potentials have been shown to yield values of the acoustic-phonon velocities that are in good agreement with measured data.[20, 21] All the RNEMD simulations are performed with the large-scale atomic/molecular massively parallel simulator (LAMMPS) package,[23] which has successfully simulated graphene monolayers in our previous studies.[24-27]

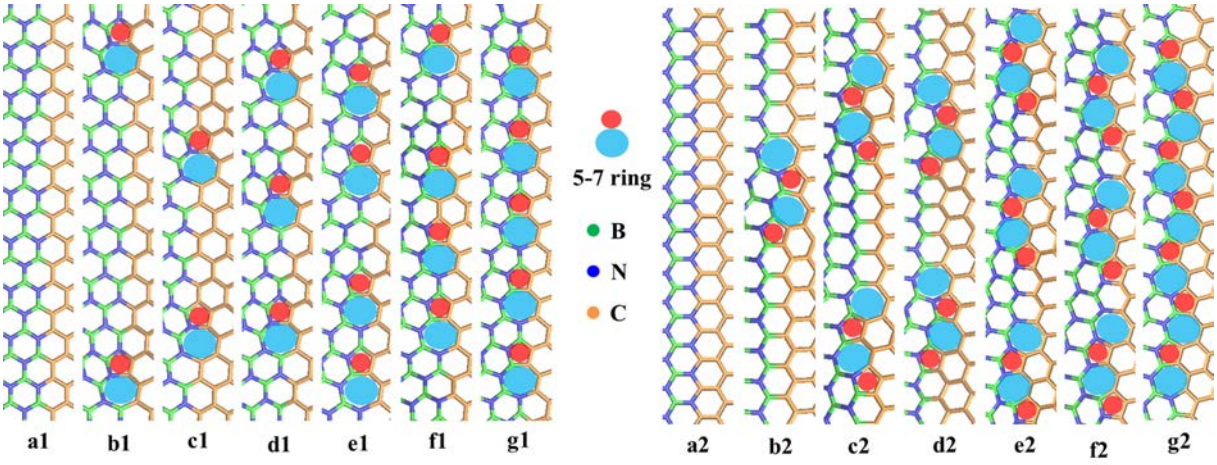

Fig. 2. Tilt grain boundary structures of zigzag-oriented GBs with θ_{zigzag} values of (a1) 0°, (b1) 5.1°, (c1) 9.4°, (d1) 13.2°, (e1) 16.4°, (f1) 17.9°, (g1) 21.8°, and armchair-oriented GBs with $\theta_{armchair}$ values of (a2) 0°, (b2) 9.5°, (c2) 13.2°, (d2) 15.2°, (e2) 17.9°, (f2) 21.8°, (g2) 27.8°.

G/h-BN heterostructures are firstly energetically minimized and applied with an external pressure tensor, in order to obtain the final structures with minimum potential energy and specified pressure tensor. RNEMD simulations are then carried out on the relaxed structures at room temperature (T=300 K) in a microcanonical NVE ensemble for 22.5 ns, with a time step of 0.5 fs. After the steady state regime is reached, the temperature profile through the

structures is determined by averaging over 2.5 ns, by dividing the structure into slabs of about 8 Å wide.

Firstly, we discuss the influence of misorientation angles on the grain boundary energies of G/h-BN heterostructures, as shown in Fig. 3(a). For values of θ_{zigzag}=0° and θ_{zigzag}=60° (refer to pure zigzag- and armchair-oriented GBs), grain boundary energy γ is non-zero, which is different from γ=0 in polycrystalline graphene.[28, 29] This is because that there exists lattice mismatch between initial graphene and h-BN grains. Thus, extra energy is needed to fully relax such lattice mismatch. As for values of θ_{zigzag} less than 17.9° and more than 42.1° (refer to smaller zigzag and armchair misorientation angles), γ gets increased with respect to θ_{zigzag}. This can be attributed to the increase of lattice mismatch. When values of θ_{zigzag} between 17.9° and 42.1° (refer to larger zigzag and armchair misorientation angles), γ surprisingly gets decreased and reaches to local minimum values at θ_{zigzag}=21.8° and θ_{zigzag}=32.2°. Here, the lower values of γ are highly related to the high-symmetry GBs in G/h-BN heterostructures.[28]

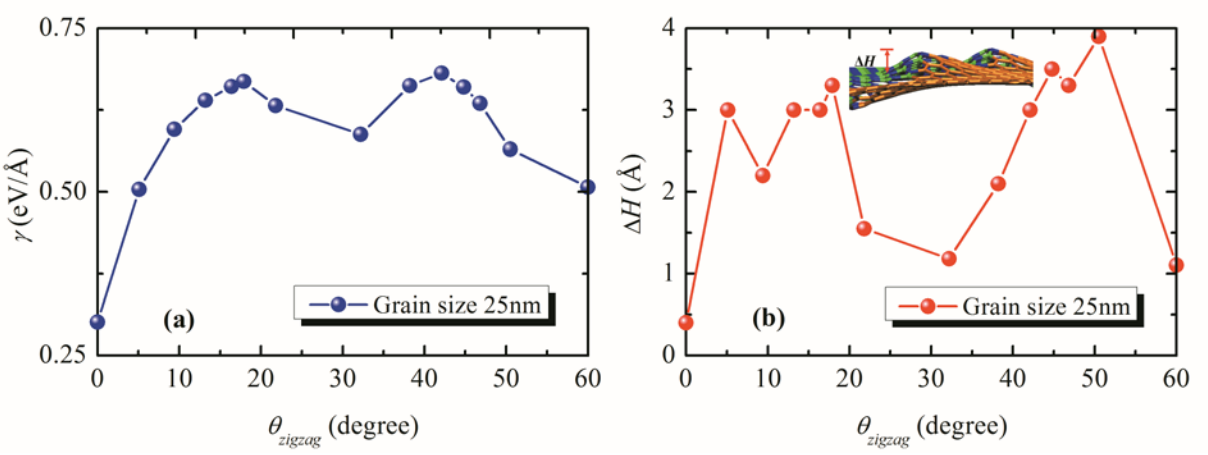

Fig. 3. (a) Grain boundary energies γ and (b) buckling magnitude ΔH as a function of zigzag misorientation angles θ_{zigzag}.

5-7 rings, which can be seen as GB dislocations, induce non-zero strain fields in G/h-BN heterostructures, and correspondingly structural buckling. Fig. 3(b) depicts the buckling magnitude ΔH as a function of θ_{zigzag}. It is interesting to notice that there are much smaller values of ΔH at θ_{zigzag}=21.8° and θ_{zigzag}=32.2°, which indicates higher densities of 5-7 rings (dislocations). This may lie in the reason that in these cases the strain fields induced by these dislocations overlap and cancel with each other, leading to smaller buckling.

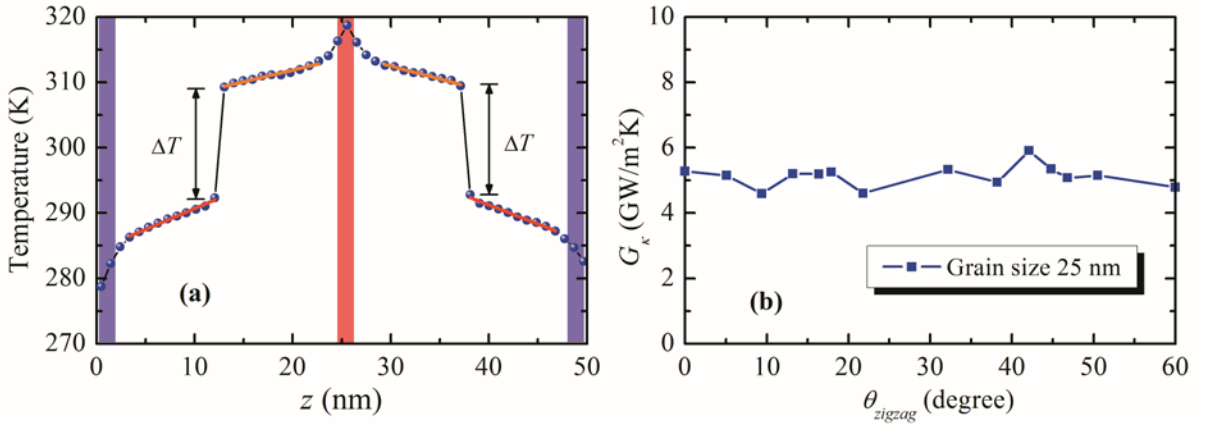

Fig. 4. (a) Steady-state temperature profile through G/h-BN heterostructure with pure zigzag-oriented GBs (θ_{zigzag}=0°). (b) Interfacial thermal conductance of tilt GBs as a function of θ_{zigzag}

We then study the thermal properties of tilt GBs in G/h-BN heterostructures. In Fig. 4(a), the average temperature profile for the heterostructure with pure zigzag-oriented GBs (θ_{zigzag}=0°) is nonlinear near the heat source and sink parts owing to finite size effects as mentioned in previous work.[30] To evaluate the thermal conductivities κ of both

graphene and h-BN grains, we determine the temperature gradient (the slope of fitted orange and red lines in Fig. 4(a)) of the middle part. In the case of θ_{zigzag}=0°, according to Eq. (2), the values of κ_G and $\kappa_{\text{h-BN}}$ are 181 and 111 W/mK, respectively. It is also found that κ_G and $\kappa_{h\text{-}BN}$ are insensitive to misorientation angles. The simulation results of κ_{G} and $\kappa_{\text{h-BN}}$ are much smaller than experimental ones. This is in that the mean free path of phonons in graphene and h-BN are more than 200 nm,[31, 32] which is much bigger than the size of our models. Therefore, besides phonon-phonon scattering, we also need consider the scattering at the heat sink and source of the heterostructures. And the thermal conductivity satisfies the relation.

Also shown in the average temperature profile (Fig. 4(a)), there is obvious temperature drop ΔT across tilt GBs in G/h-BN heterostructures. In terms of Eq. (1), the interfacial thermal conductance of tilt GBs G_κ can be determined, as presented in Fig. 4(b). It indicates that G_κ is nearly independent of misorientation angles, and has an approximately constant value of 5 GW/m^{2}K. While in the case of polycrystalline graphene, the interfacial thermal conductance of graphene GBs reduces with increasing misorientation angle, and its value is one order of magnitude larger than that of G/h-BN GBs. Such dependence on misorientation angle and higher interfacial thermal conductance in polycrystalline graphene may be due to its more symmetry structure. Thus, there is less mismatch between the phonon vibrational spectra of graphene grains than that of graphene and h-BN grains.

In summary, we have explored the energetic and thermal properties of GBs in G/h-BN heterostructures. Our simulation results indicate that lattice mismatch between graphene and h-BN grains causes non-zero GB energy of pure zigzag- (θ_{zigzag}=0°) and armchair-oriented (θ_{zigzag}=60°) GBs. We also identify two local minimum GB energies having values of θ_{zigzag}=21.8° and θ_{zigzag}=32.2°. As for thermal transport across GBs in G/h-BN heterostructures, it is found that misorientation angle has no significant influence on the interfacial thermal conductance. These results shed light onto precise synthesis of G/h-BN heterostructures.

Acknowledgement

The authors would like to acknowledge the HPC center in Queensland University of Technology (QUT) for access to its computation resources. M.C. Wang also thanks the financial support of Write-Up Scholarship from QUT.

References

1. K. S. Novoselov et al., Science, 306, 666 (2004).
2. K. S. Novoselov et al., Science, 315, 1379 (2007).
3. A. K. Geim and K. S. Novoselov, Nat Mater, 6, 183 (2007).
4. K. Watanabe et al., Nat Mater, 3, 404 (2004).
5. M. Topsakal et al., Phys Rev B, 79, 115442 (2009).
6. J. Qi et al., Nano Lett, 12, 1224 (2012).
7. G.-H. Lee et al., Appl Phys Lett, 99, 243114 (2011).
8. L. Britnell et al., Nano Lett, 12, 1707 (2012).
9. M. P. Levendorf et al., Nature, 488, 627 (2012).
10. Z. Liu et al., Nat Nano, 8, 119 (2013).
11. L. Ci et al., Nat Mater, 9, 430 (2010).
12. J. He et al., Appl Phys Lett, 97, 193305 (2010).
13. J. Li and V. B. Shenoy, Appl Phys Lett, 98, 013105 (2011).
14. J. M. Pruneda, Phys Rev B, 81, 161409 (2010).
15. E. T. Swartz and R. O. Pohl, Rev Mod Phys, 61, 605 (1989).
16. S. Lin and M. J. Buehler, Nanotechnology, 24, 165702 (2013).
17. S. Lin and M. J. Buehler, Carbon, 77, 351 (2014).
18. M. Wang et al., Int J Smart Nano Mater, 5, 123 (2014).
19. F. Müller-Plathe, ChemPhysChem, 3, 754 (2002).
20. L. Lindsay and D. A. Broido, Phys Rev B, 81, 205441 (2010).
21. C. Sevik et al., Phys Rev B, 84, 085409 (2011).
22. C. Sevik et al., Phys Rev B, 86, 075403 (2012).
23. S. Plimpton, J Comput Phys, 117, 1 (1995).
24. M. C. Wang et al., Comput Mater Sci, 54, 236 (2012).
25. M. C. Wang et al., J Nano Research, 23, 43 (2013).
26. M. C. Wang et al., Comput Mater Sci, 68, 138 (2013).
27. M. Wang et al., Comput Mater Sci, 75, 69 (2013).
28. T.-H. Liu et al., Carbon, 49, 2306 (2011).
29. Y. Wei et al., Nature Materials, 11, 759 (2012).
30. P. K. Schelling et al., Phys Rev B, 65, (2002).
31. C. W. Chang et al., Phys Rev Lett, 97, (2006).
32. S. Ghosh et al., Appl Phys Lett, 92, (2008).